ATMOSPHERIC SCIENCE LETTERS
Atmos. Sci. Let. **16**: 425–431 (2015)
Published online 19 March 2015 in Wiley Online Library
(wileyonlinelibrary.com) **DOI:** 10.1002/asl2.575

RMetS
Royal Meteorological Society

The impact of extratropics-arctic-seesaw of perturbation potential energy on surface air temperature in boreal winters

Lei Wang,[1,2] Zhanggui Wang,[1]* Jianping Li[3] and Fei Zheng[4]

[1]*Key Laboratory of Research on Marine Hazards Forecasting, National Marine Environmental Forecasting Center, Beijing, China*
[2]*School of Physics, Peking University, Beijing, China*
[3]*College of Global Change and Earth System Science, Beijing Normal University, China*
[4]*State Key Laboratory of Numerical Modeling for Atmospheric Sciences and Geophysical Fluid Dynamics, Institute of Atmospheric Physics, Chinese Academy of Sciences, Beijing, China*

**Correspondence to:*
Dr Z. Wang, National Marine Environmental Forecasting Center, No.8, Dahuisi Street, Haidian District, Beijing, China 100081.
E-mail: zgwang@nmefc.gov.cn

Received: 18 March 2014
Revised: 27 August 2014
Accepted: 16 February 2015

Abstract

Seesaw pattern of the perturbation potential energy in the extratropics and the Arctic (defined as PEAS) is observed. The PEAS is closely related to the Arctic Oscillation, kinetic energy and zonal wind in the middle- and high-latitude. The PEAS may influence atmospheric circulation via northern migration of anomalous Ferrel cell, accompanying by suppressed subtropical jet stream and enhanced polar jet stream. Anomalous warm conditions associated with the PEAS are observed in high-latitude of Eurasia, whereas cold anomalies are presented in Greenland, northeast Africa and southwest China, which is mainly attributed to the horizontal temperature advection.

Keywords: perturbation potential energy; kinetic energy; surface air temperature; Arctic Oscillation; Ferrel cell

1. Introduction

The amount and distribution of energy exert profound influence on weather and climate on earth (Trenberth *et al.*, 2009), and solar radiation absorbed by climate system is transformed into sensible heat, latent heat, potential energy and kinetic energy (KE), accompanying the evolving of a wide variety of weather phenomenon. The concept of available potential energy (APE) was introduced by Lorenz (1955) and then applied to assess energy efficiency (Smith, 1969a, 1969b; Johnson, 1970; Edmon, 1978; Gu, 1990). It extensively expanded the knowledge of evolution of atmospheric circulation, which consisted of the generation of APE via diabatic heating, energy conversion between APE and KE and the dissipation of KE through friction (Lorenz, 1960, 1978; van Mieghem, 1973; Peixoto and Oort, 1992; Huang, 2005).

Although previous studies on APE have made great progresses in understanding the efficiency of energy conversion on global scale, the application of APE on a local scale is inappropriate because the formula of APE is based on global-averaged variables; improvements are required to be made when applying APE on a local scale. Li and Gao (2006) introduced the concept of perturbation potential energy (PPE), which indicates the maximum amount of total potential energy that could be converted into KE in local scale, and notably PPE is more strongly coupled to KE than does APE. According to Gao and Li (2012), the leading coupled modes of extratropical PPE and KE are also the dominant modes in their own variability, and PPE has also a tense relation with atmospheric low frequency variability modes such as annular modes. The PPE is also applied to investigate the variability of the South China Sea summer monsoon (Wang *et al.*, 2012, 2013).

Generally, PPE is characterized by zonal distribution (Gao, 2006; Wang *et al.*, 2013), and Wang *et al.* (2014) investigated the relationship between PPE, KE and El Niño-Southern Oscillation (ENSO). Notable seesaw of first-order PPE (PPE1) was observed between the extratropics and the Arctic in boreal winters (Figure 1(a)). It is well known that the Arctic Oscillation (AO) is the primary mode of low frequency variability in the extratropics of Northern Hemisphere, and the AO affects climate and weather over broad regions in the Northern Hemisphere (Hurrel, 1995, 1996; Thompson and Wallace, 1998, 2001; Wu and Huang, 1999; Higgins *et al.*, 2000, 2001; Gong *et al.*, 2001; Li and Wang, 2003a; Seager *et al.*, 2010). In recent boreal winters, North America (in 2013/2014), European (in 2009/2010) and China (in 2007/2008) have undergone extreme cold events which cause severe losses of property. As both of them occur in extratropical atmosphere, the relationship between the seesaw of PPE1 and the AO as well as regional climate is of great scientific interest, which is the main scope of this work.

2. Data and methodology

This study employs the NCEP-DOE Reanalysis 2 monthly datasets for January 1979 to February 2013

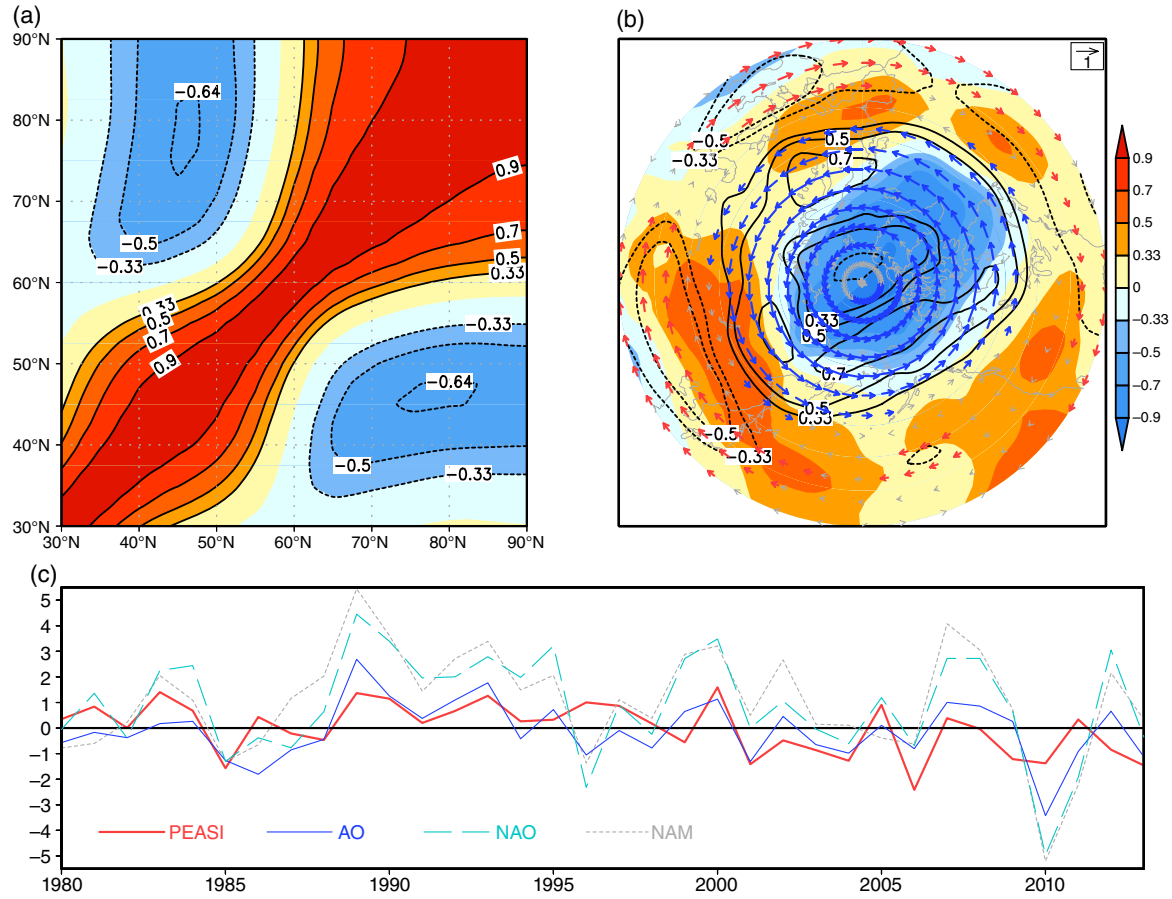

Figure 1. (a) Cross correlations between zonally averaged PPE1 anomalies in DJF; (b) correlation maps between PEASI and PPE1 (shading), between PEASI and KE (contours), between PEASI and 1000–100 hPa vertically averaged zonal wind (vector) in DJF; (c) normalized time series of PEASI, AO, NAO and NAM. The thick red/blue vectors in (b) indicate significant at the 95% confidence level, the thin gray vectors are used for lower confidence levels and the outmost latitude is 30°N.

(Kanamitsu *et al.*, 2002), which include temperature, wind, geopotential height, surface pressure on a 2.5°×2.5° grid, 2-m air temperature and 10-m horizontal wind on a Gaussian grid.

The monthly AO index is derived from Climate Prediction Center (CPC)/National Centers for Environmental Prediction (NCEP)/National Oceanic and Atmospheric Administration (NOAA) (Higgins *et al.*, 2000, 2001): http://www.cpc.ncep.noaa.gov/products/precip/CWlink/daily_ao_index/month_ao_index.shtml. The monthly Northern Hemisphere Annular Mode (NAM) index and North Atlantic Oscillation (NAO) index are obtained from (Li and Wang, 2003a, 2003b) http://ljp.lasg.ac.cn/dct/page/65544.

To provide a theoretical background of this work, the basic concept of PPE is briefly reviewed here. Li and Gao (2006) proposed a new concept called PPE, which could be expressed as:

$$P'_{Li} = \frac{p_{00}^{(i-1)\kappa}\prod_{j=0}^{i-1}(1+\kappa-j)}{i!r_d(1+\kappa)} \int_0^{p_s} \frac{T'^i}{p^{(i-1)(1+\kappa)}}\left(-\frac{\partial\overline{\theta}}{\partial p}\right)^{-i+1} dp \qquad (1)$$

where i is the order of PPE, p is pressure, p_s is surface pressure and p_{00} is reference pressure (usually taken as 1000 hPa). Here, also g is gravity acceleration, R is gas constant of dry air, c_p is specific heat at constant pressure, while $r_d = g/c_p$ is the dry adiabatic lapse rate and $\kappa = R/c_p$. Additionally, T is temperature, $\overline{T}$ is a global average on isobaric surface, T' is the departure from this global average and $\theta$is potential temperature. The mathematical formulas for first-order PPE (PPE1) and second-order PPE (PPE2) are listed as follows:

$$\mathrm{PPE1} = \frac{1}{r_d}\int_0^{p_s} T'dp \qquad (2)$$

$$\mathrm{PPE2} = \frac{\kappa p_{00}^{\kappa}}{2r_d}\int_0^{p_s}\frac{T'^2}{p^{1+\kappa}}\left(-\frac{\partial\overline{\theta}}{\partial p}\right)^{-1} dp \qquad (3)$$

The global average of PPE1 is zero, which does not mean it plays little role in atmospheric circulation, whereas the global averaged PPE2 is equal to traditional APE, and note that PPE1 generally exceeds PPE2 on a regional scale. In reality, APE and PPE represent available energy on global and local scale, respectively. We focus on the characteristics of PPE1 in this study.

Wang *et al.* (2012) derived the governing equations of PPE1 and KE, which are briefly introduced below:

$$\frac{\partial}{\partial t}\mathrm{PPE1} = \mathfrak{T}_L + \aleph_L + R_L - CK + G_L \qquad (4)$$

$$\frac{\partial}{\partial t}\mathrm{KE} = B_K + \mathfrak{R}_K + C_K + M_K \qquad (5)$$

where $\mathrm{KE} = g^{-1}\int_0^{p_s} 0.5\ \left(u^2+v^2\right)\ dp$ is KE. $C_K = g^{-1}\int_0^{p_s} \omega\left(\partial\phi'/\partial p\right)dp$ represents a conversion term between PPE1 and KE, which depends on vertical velocity and atmospheric stability. Here also $G_L = g^{-1}\int_0^{p_s} Q'dp$ represents the source (sink) term of PPE1, which depends on non-uniform diabatic heating. While $M_K = g^{-1}\int_0^{p_s} \overrightarrow{V_h}\overrightarrow{\Upsilon_h}dp$ represents viscous dissipation with $\overrightarrow{V_h}$ the horizontal velocity vector and $\overrightarrow{\Upsilon_h}$ the horizontal friction force. Additionally, $\mathfrak{T}_L$ and B_K represent horizontal boundary terms. Moreover, $\aleph_L$, R_L and $\mathfrak{R}_K$ represent topographically induced terms (Appendix S1, supporting information). More details on the derivation of PPE and related governing equations are available in the Supporting Information of Wang *et al.* (2014).

Linear regression, correlation and composite analysis are employed in this work. Composite analysis for years of anomalously high and low index is defined by deviations exceeding one standard deviation of the year-to-year variability. All results based on the boreal winters season, defined here as December to February (DJF). Prior to analysis, all variables, such as PPE1, are calculated for each month and then converted to winter means.

3. Results

3.1. PPE extratropics Arctic seesaw

Figure 1(a) shows the cross correlations of zonally averaged PPE1 anomalies in boreal winters. The most prominent feature is the negative correlations between PPE1 in the extratropics/midlatitude (40°–50°N) and that in the Arctic zone (65°–90°N). The strongest correlations occur between PPE1 over 45°N and that over 75°N. This reveals a striking north–south seesaw pattern with opposing polarities between PPE1 in extratropics/midlatitude and that in the Arctic, and implies that an increase in PPE1 in the midlatitude is associated with a decrease in the Arctic, and vice versa. To investigate further the seesaw pattern of PPE1, an index of the PPE1 extratropics Arctic seesaw (PEAS) is defined as:

$$\mathrm{PEASI} = \left(\langle\mathrm{PPE1}\rangle_{45°\mathrm{N}} - \langle\mathrm{PPE1}\rangle_{75°\mathrm{N}}\right)/2 \qquad (6)$$

where the angle brackets indicate zonal mean values. The positive PEASI is characterized by enhanced PPE1 in the extratropics and suppressed PPE1 in the Arctic.

The spatial features of the PEAS are illustrated by the correlation map between the PEASI and PPE1 (Figure 1(b)). Note that positive PPE1 anomalies appear in the midlatitude (35°–60°N) and negative PPE1 anomalies appear in the Arctic (60°–90°N), except in North America-Atlantic sectors where the negative PPE1 extends further toward midlatitude (50°–90°N). In contrast, reduced KE anomalies associated with the PEASI are observed in the midlatitude (30°–45°N), whereas enhanced KE anomalies are observed in high-latitude (50°–80°N). In addition, there are striking north–south contrasts in the PEASI-related zonal wind between midlatitude easterlies (30°–45°N) and high-latitude westerlies (55°–80°N), and the results are consistent with the anomalous patterns of KE. The spatial distribution of anomalous KE bears large similarity with the anomalous patterns of PPE1 but with the sign reversed, suggesting that KE may be regulated by PPE1 by means of energy conversions between them. Note also that the maximum KE tends to shift into transition regions of the positive and negative PPE1 anomalies, and this is possibly due to the higher efficiency of conversion from PPE1 to KE in the transition regions (Gao and Li, 2012).

Because the zonal wind in the midlatitude is usually depicted by zonal index (Rossby *et al.*, 1939; Namias, 1950; Li and Wang, 2003a) and is regulated by AO/NAM/NAO (Thompson and Wallace, 1998, 2000; Li and Wang, 2003b), the significant correlation between midlatitude zonal wind and the PEASI suggests that the PEAS may be linked with AO. To test this assertion, Figure 1(c) displays the normalized time series of the PEASI, AO, NAM and NAO in DJF. Of note is that the PEASI is highly correlated with AO and NAO, to a less degree with NAM, the corresponding coefficients are 0.55, 0.51 and 0.42, all of which are statistically significant at the 95% confidence level. The correlation pattern between the PEASI and KE gives a more zonally symmetric appearance than that of the AO and KE (Figure not shown), especially over high-latitude regions of Asia and North America. In addition, the negative correlation between the PEASI and KE covers more of the entrance area of East Asia subtropical jet.

The PEASI captures the hemispheric features of the seesaw of PPE1 between extratropics and the Arctic faithfully. Moreover, the PEAS is closely related to middle- and high-latitude KE and zonal wind in boreal winters.

3.2. Physical features related to the PEAS

In this section, we investigate the vertical structure of atmospheric circulation associated with the PEAS and explore the physical linkage between the PEAS and AO. As indicated in Figure 2(a), the correlation patterns of zonally averaged meridional circulation associated with the PEASI are marked by the anomalous Ferrel cell centered on 60°N, about 10° north of the climatological location of Ferrel cell (means from 1979

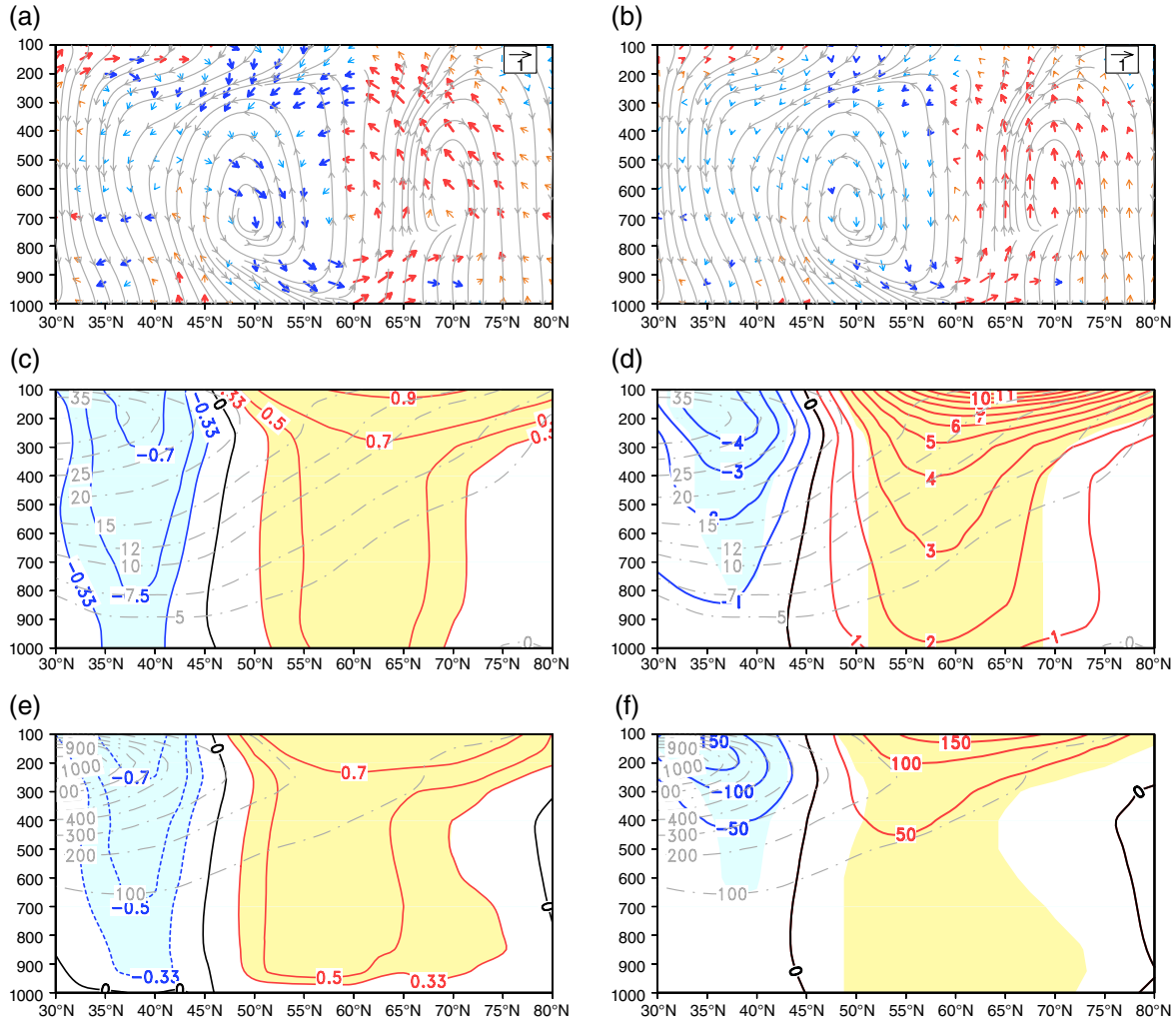

Figure 2. Correlation coefficients between PEASI and zonally averaged (a) meridional circulation (vectors); (c) zonal wind, (e) KE. (b, d, f) are same as (a, c, e) but for composite differences patterns (units: m s^{-1}, -10^{-2} P s^{-1}; m s^{-1}; J kg^{-1}). The thick red/blue (thin orange/light) vectors in (a)–(b) indicate significant (insignificant) at the 95% confidence level, shading in (c)–(f) indicates significant at the 95% confidence level. Climatological zonal averaged meridional circulation (gray streamline) are shown in (a), (b); zonal wind (gray-dashed line) in (c), (d); KE (gray-dashed line) in (e), (f), respectively.

to 2012), indicating poleward movement of the Ferrel cell. The anomalous Ferrel cell consists of a strong ascent flow poleward of 60°N with a maximum near 65°N, a downwelling flow over 35°–57.5°N with a minimum near 50°N, a near-surface southerly flow accompanying by an upper-troposphere northerly flow over 50°–70°N. Composite analysis (Figure 2(b)) reveals the strong ascent emerges at 65°N but descent at 35°–57.5°N, and together with the low-level southerly and the high-level northerly, they compose the anomalous Ferrel cell. The locations of the anomalous and climatological Ferrel cell are suggestive of northern migration of the Ferrel cell. Note also that, there appears to be an anomalous shallow tropical cell over 40°–50°N, south of the downwelling branch of the anomalous Ferrel cell, resulting in weakening of the equator branch of Ferrel cell (Figure 2(a) and (b)). Furthermore, the powerful southerly over 50°–70°N brings heat from midlatitude to polar regions, which weakens the polar cell through raising surface temperature in the Arctic region.

Predominant features in Figure 2(c) are easterly anomalies between 30° and 45°N in contrast to westerly anomalies between 45° and 70°N, which are suggestive of a suppressed subtropical jet stream with an enhancement polar jet stream. As can be seen in Figure 2(d), easterly anomalies develop in the subtropics (30°–45°N) whereas westerly anomalies develop in high-latitude (50°–75°N). The robust relationship between the PEASI and westerly in high-latitude (50°–70°N) indicates that the PEASI is a valuable indicator for the intensity of zonal wind within the range.

The distribution of KE anomalies associated with the PEASI (Figure 2(e) and (f)) is consistent with the anomalous pattern of zonal wind, implying that energetics approach is an alternative way in studies of circulation variability in the extratropics. As can be seen in Figure 2(e), KE correlates negatively with PEASI in the subtropics (30°–45°N) and positively in the high-latitude (50°–75°N). This indicates that when PPE1 increase in the extratropics (40°–50°N)

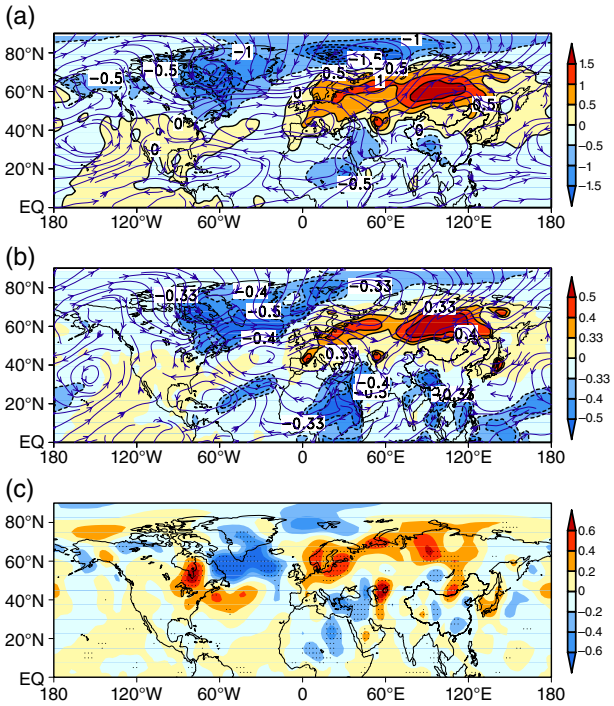

Figure 3. (a) Regression patterns of 850 hPa horizontal wind (streamline) and 2 m temperature (shading) on PEASI in DJF (1979–2012) (units: ms^{-1}/PEASI, °C/PEASI), (b) same as (a) but for correlation patterns of PEASI, (c) composite difference of the horizontal temperature advection integrated from 1000 to 600 hPa for years of anomalously high and low PEASI exceeding one standard deviation (units: $°C\,s^{-1}$).

and decrease in the Arctic (65°–90°N), namely, in the positive polarity of PEASI, KE is apt to increase in high-latitude and decrease in the subtropics. The features of KE are reproduced in Figure 2(f). The counter relationship between KE and PPE1 is possible due to energy conversion between them, and further investigation is deserved to uncover that question.

3.3. Relationship between the PEAS and surface air temperature

Having documented that the PEAS affects atmospheric circulation, the influence of the PEAS on climate such as surface air temperature (SAT) remains unclear and thus needs to be examined.

A regression map of SAT anomalies onto the PEASI in boreal winters is presented in Figure 3(a); the positive temperature anomalies are located in Eurasia and United States, whereas the negative temperature anomalies are located in Greenland, northeast Africa and southwest China. This indicates that a positive phase of the PEASI is associated with anomalous warmer across Eurasia and United States, and colder than normal conditions in Greenland, northeast Africa and southwest China. Figure 3(b) depicts the correlation pattern between the PEASI and SAT. Significant positive correlations are found across Eurasia along 50° and 65°N, while cold anomalies are presented in Baffin Island, northeast Africa and southwestern China. Note that in southwestern China, South Asia and eastern Africa, there appears to be significant negative correlations between SAT and the PEASI, whereas the correlation with AO (Figure not shown) is insignificant.

To examine further the mechanism of the impacts of the PEAS on SAT, Figure 3(c) describes the composite difference patterns of the horizontal temperature advection for the anomalous high and low PEASI. The cold advections are observed in Greenland, middle of North Africa and southwestern China, which are similar to the distributions of the cold anomalies (Figure 3(a)), suggesting that the horizontal temperature advections are largely responsible for the anomalous patterns of SAT. In contrast, the warm advections are presented in North European Plain, Siberia Plateau and midlatitude Atlantic that favors the anomalous warm in Eurasia and midlatitude Atlantic. Although there are some discrepancies between the pattern of anomalous horizontal temperature advection and that of SAT in James Bay, overall, the pattern of horizontal temperature advection is consistent with the distribution of SAT, indicating it may play a critical role in maintaining the anomalous pattern of SAT.

The horizontal temperature advections are closely linked to the horizontal wind fields which are regulated by the high and low pressure systems. Figure 4(a) displays that jet stream intensifies from Labrador to Scandinavia accompanying by the deepening Iceland Low and enhanced Azores High (Figure 4(b)), resulting in the changes of strength (wind direction) in Atlantic and European, and thus to changes of horizontal temperature advection and SAT. In addition, the enhanced Siberian High leads to anomalous northeasterly blowing to southern China and the occurrence of cold anomalies in southwest China. The correlation patterns of height and wind fields (Figure 4 (c) and (d)) are consistent with the composite analysis (Figure 4 (a) and (b)), and this provides assurance for the confidence of the results.

4. Conclusion and discussion

In this paper, we presented observational evidences for the seesaw pattern in wintertime PPE1 between the extratropics and the Arctic (PEAS), and the PEAS indicates out-of-phase relations between PPE1 in the extratropics and that in the Arctic. Associated with the PEAS, anomalous Ferrel cell locates at high-latitude about 10° north of its climatological normal accompanying by enhanced high-latitude westerly and weakened easterly equatorward of 45°N. Under the action of Ferrel cell, the PEAS is closely linked to AO/NAO/NAM. The warming across Eurasia and the cooling in Greenland, northeast Africa and southwest China result from the changes in the PEAS, which cause the changes of temperature advection through changes of atmospheric action centers.

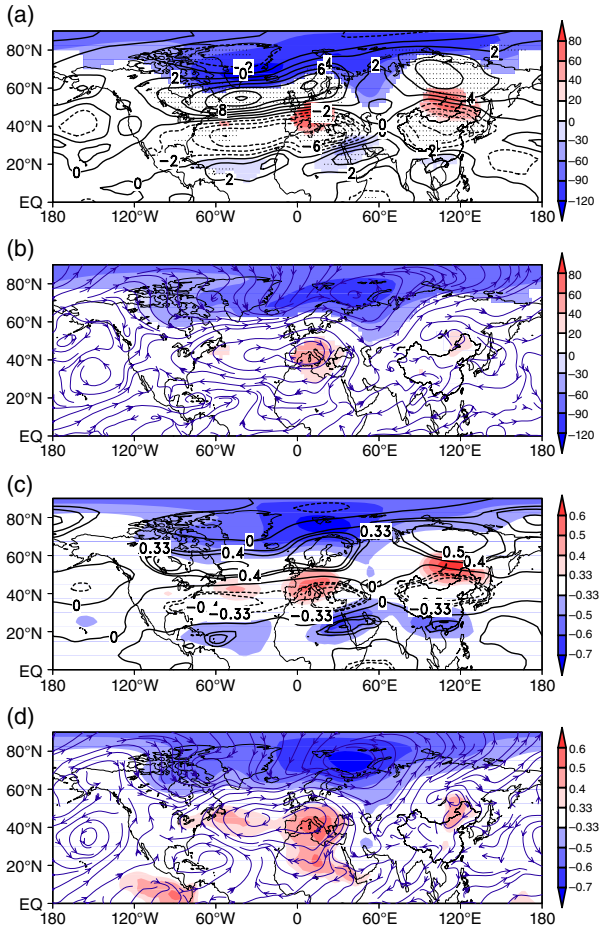

Figure 4. Composite difference of (a) 500-hPa height (shading, units: gpm) and 300-hPa zonal horizontal wind (contours, units: $m\,s^{-1}$) (b) 850-hPa height (shading, units: gpm) and horizontal wind (streamline) between strong and weak PEASI years during DJF. Dotted areas in (a) indicate the wind difference is significant at the 95% confidence level.(c) and (d) as for (a), (b), but for correlation maps, shading in (a)–(d) indicates significant at the 95% confidence level.

The results showed that Ferrel cell is the key factor linked to the PEAS, which is reminiscent of the anomalous Ferrel cell associating with NAM (Li and Wang, 2003a). In reality, it shares more similarity with the anomalous circulation pattern associated with AO (not shown). Moreover, the zonal index (Rossby *et al.*, 1939) is featured by the high-latitude zonal wind, coincidentally the PEAS is highly correlated with high-latitude zonal wind, possibly as a result of the energy conversion between PPE and KE supported by the significant negative correlation between them. Although the PEAS-related anomalous temperature in Midwest Canada is opposite to that of NAO (Wang *et al.*, 2010), there are more similarity between the impacts of the PEAS on SAT with that of the NAO (Hurrel, 1996). It seems to be rational that the intense relations occur between PEAS and surface temperature, for PPE in essence depends on the hemispheric distribution of temperature.

Our results may provide a new avenue for exploring the extratropical atmospheric variability. Further studies on relationship between the PEAS and the AO are particularly enlightening for understanding the energetics of the AO. Additionally, the PEAS may have profound influence on precipitation in the Northern Hemisphere and that will be investigated in future work.

Acknowledgements

This work was jointly supported by the National Basic Research Program of China (2010CB950303), the National Natural Science Foundation of China (41375110), the China Special Fund for Meteorological Research in the Public Interest (GYHY201506030). Thanks to the editor Dr Helen Dacre and the three anonymous reviewers for their comments and suggestions that helped us to improve the manuscript.

Supporting information

The following supporting information is available:

Appendix S1. The derivation of perturbation potential energy and its governing equations.

References

Edmon HJ. 1978. A reexamination of limited area available potential energy budget equations. *Journal of the Atmospheric Sciences* **35**(9): 1655–1659.

Gao L. 2006. Theoretical Studies and Diagnostic Analyses of Perturbation Potential Energy. PhD dissertation, Institute of Atmospheric Physics, Chinese Academy of Sciences: Beijing; 1–33 (in Chinese).

Gao L, Li JP. 2012. Relationship and mechanism between perturbation potential energy and atmospheric general circulation anomalies. *Chinese Journal of Geophysics* **55**(3): 359–374.

Gong DY, Wang SW, Zhu J. 2001. East Asian winter monsoon and Arctic Oscillation. *Geophysical Research Letters* **28**: 2073–2076.

Gu XZ. 1990. A theoretical study of the available potential energy in a limited atmospheric region. *Acta Meteorologica Sinica* **48**(2): 248–252 (in Chinese).

Higgins RW, Leetmaa A, Xue Y, Barnston A. 2000. Dominant factors influencing the seasonal predictability of U.S. Precipitation and surface air temperature. *Journal of Climate* **13**: 3994–4017.

Higgins RW, Zhou Y, Kim HK. 2001. Relationships between El Nino-Southern Oscillation and the Arctic Oscillation: a Climate-Weather Link. NCEP/Climate Prediction Center ATLAS No. 8. http://www.cpc.ncep.noaa.gov/research_papers/ncep_cpc_atlas/8/index.html; http://www.cpc.ncep.noaa.gov/research_papers/ncep_cpc_atlas/8/toc.html (accessed 11 March 2015).

Huang RX. 2005. Available potential energy in the world's oceans. *Journal of Marine Research* **63**: 141–158.

Hurrel JW. 1995. Decadal trends in the North Atlantic osciallation: regional temperatures and precipitation. *Science* **269**: 676–679.

Hurrel JW. 1996. Influence of variations in extratropical wintertime teleconnections on Northern Hemisphere temperature. *Geophysical Research Letter* **23**: 665–668.

Johnson DR. 1970. The available potential energy of storms. *Journal of the Atmospheric Sciences* **27**(5): 727–741.

Kanamitsu M, Ebisuzaki W, Woollen J, Yang SK, Hnilo JJ, Fiorino M, Potter GL. 2002. NCEP-DEO AMIP-II Reanalysis (R-2). *Bulletin of the American Meteorological Society* **83**: 1631–1643.

Li JP, Gao L. 2006. Theory on perturbation potential energy and its applications – concept, expression and spatiotemporal structures of PPE. *Chinese Journal of Atmospheric Sciences* **30**(5): 834–848.

Li JP, Wang JXL. 2003a. A modified zonal index and its physical sense. *Geophysical Research Letter* **30**(12): 1632.

Li JP, Wang JXL. 2003b. A new North Atlantic Oscillation index and its variability. *Advance in Atmospheric Science* **20**(5): 661–676.

Lorenz EN. 1955. Available potential energy and the maintenance of the general circulation. *Tellus* **7**: 157–167.

Lorenz EN. 1960. Generation of available potential energy and the intensity of the general circulation. In *Dynamics of Climate*, Pfeffer RC (ed). Pergamon Press: Oxford, UK; 86–92.

Lorenz EN. 1978. Available energy and the maintenance of a moist circulation. *Tellus* **30**: 15–31.

van Mieghem J. 1973. *Atmospheric Energetics*. Clarendon Press: Oxford, UK.

Namias JC. 1950. The index cycle and its role in the general circulation. *Journal of Meteorology* **7**: 130–139.

Peixoto JP, Oort AH. 1992. *Physics of Climate*Chapter 14. American Institute of Physics Press: New York, NY.

Rossby CG and Collaborators. 1939. Relations between variations in the intensity of the zonal circulation of the atmosphere and displacements of the semi-permanent centers of action. *Journal of Marine Research* **2**: 38–55.

Seager R, Kushnir Y, Nakamura J, Ting M, Naik N. 2010. Northern Hemisphere winter snow anomalies: ENSO, NAO and the winter of 2009/10. *Geophysical Research Letter* **37**: L14703.

Smith PJ. 1969a. On the contribution of a limited region to the global energy budget. *Tellus* **21**: 202–207.

Smith PJ. 1969b. A computational study of the energetics of a limited region of the atmosphere. *Tellus* **21**: 193–201.

Thompson DWJ, Wallace JM. 1998. The Arctic Oscillation signature in the wintertime geopotential height and temperature fields. *Geophysical Research Letter* **25**: 1297–1300.

Thompson DWJ, Wallace JM. 2000. Annular modes in the extratropical circulation. Part I: month-to-month variability. *Journal of Climate* **13**: 1000–1016.

Thompson DWJ, Wallace JM. 2001. Regional climate impacts of the Northern Hemisphere annular mode. *Science* **293**: 85–89.

Trenberth KE, Fasullo JT, Kiehl JT. 2009. Earth's global energy budget. *Bulletin of the American Meteorological Society* **90**: 311–323.

Wang C, Liu H, Lee SK. 2010. The record-breaking cold temperatures during the winter of 2009/2010 in the Northern Hemisphere. *Atmospheric Science Letters* **11**: 161–168.

Wang L, Li JP, Guo Y. 2012. Governing equations of atmospheric layer perturbation potential energy and its applications, energy budget of the South China Sea summer monsoon activity. *Chinese Journal of Atmospheric Sciences* **36**(4): 769–783.

Wang L, Li JP, Ding RQ. 2013. Theory on layer perturbation potential energy and its applications – cases study on annual variation of the South China Sea summer monsoon. *Chinese Journal of Geophysics* **56**(2): 392–408.

Wang L, Li JP, Wang ZG, Li YJ, Zheng F. 2014. The oscillation of the perturbation potential energy between the extratropics and tropics in boreal winter. *Atmospheric Science Letters*, doi: 10.1002/asl2.532.

Wu BY, Huang RH. 1999. Effects of the extremes in the North Atlantic Oscillation on East Asia winter monsoon. *Chinese Journal of Atmospheric Sciences* **23**(6): 641–651.

